Electronic Supplementary Material (ESI) for Chemical Communications.


# Supporting Information

*for*

# Enhancing the carbon capture capacities of a rigid ultra-microporous MOF through gate-opening at low $CO_2$ pressures assisted by swiveling oxalate pillars

Aparna Banerjee,[a] Shyamapada Nandi,[a] Parveen Nasa[a] and Ramanathan Vaidhyanathan [a]*

[†]Department of Chemistry, Indian Institute of Science Education and Research (IISER) Pune, Dr. Homi Bhabha Road, Pune, India - 411008

* vaidhya@iiserpune.ac.in.

## *Contents*

## 1. Materials and methods

All the organic chemicals were purchased from sigma aldrich. The nickel salts were procured from Alfa Aesar. Compounds and solvents were all used without any further purification.

All synthesis employed $ZnCO_3$, Oxalic acid and 3-aminotriazole in the ratio 1:1:5 and the solvothermal reactions were carried out at 180 $^oC$ for 2 days.

$Zn_2(C_2O_4)(C_2N_4H_3)_2.(H_2O)_x$(**2**): In a typical synthesis of **2**, Zn salt, oxalic acid and 3-amino-1,2,4-triazole were added in a 1:1:5 molar ratio in to $H_2O$ (5ml), in a 23ml autoclave, which was stirred for 30 minutes at room temperature and then was reacted solvothermally at 180 °C for 2 days. On cooling, colorless microcrystalline sample was obtained. Product was then washed with copious amounts of $H_2O$ and MeOH to remove any unreacted organics and then dried in air.

$Zn_4(C_2O_4)_2(C_2N_4H_3)_4.(EtOH)_2.(H_2O)$ (**3**): **3** was synthesized in a mixed solvent medium. In a typical synthesis, Zn salt, oxalic acid and 3-amino-1,2,4-triazole were added in a 1:1:5 molar ratio in to 1ml $H_2O$+ 5ml EtOH, in a 23ml autoclave, which was stirred for 30 minutes at room temperature and then was reacted solvothermally at 180 °C for 2 days. On cooling, colorless crystals suitable for single crystal x-ray diffraction were obtained. Product was then washed with copious amounts of $H_2O$ and MeOH to remove any unreacted organics and then dried in air.

$Zn_2(C_2O_4)(C_2N_4H_3)_2.$(1-PrOH) (**4**): **4** was synthesized using synthetic procedure comparable to those used for **3**, by replacing ethanol by same amount of 1-Propanol.

$Zn_2(C_2O_4)(C_2N_4H_3)_2.$(solvent)(**2***): **2*** synthesized hydrothermally using synthetic procedure comparable to those used for **2**. Solvent in this case was 3ml $H_2O$ + 3ml BuOH.

Note: Phase 2/2* could be synthesized using single solvent reactions involving BuOH, however, this does not yield large enough single crystals for x-ray diffraction.

Use of 1ml $H_2O$ + Solvent (Solvent = pentanol, hexanol, heptanol) yielded 2/2* as microcrystalline solids. This suggests all aliphatic alcohols bulkier than butanol could act as templates for synthesis of **2**.

## 2. Analytical characterizations

*Powder X-ray diffraction:*

Powder XRDs were carried out using a Rigaku Miniflex-600 instrument and processed using PDXL software.

*Thermogravimetric Analysis:*

Thermogravimetry was carried out on NETSZCH TGA-DSC system. The routine TGAs were done under $N_2$ gas flow (20 ml $min^{-1}$) and samples were heated from RT to 550 $^{\circ}C$ at 2 K $min^{-1}$.

*IR spectroscopy:*

IR spectra were obtained using a Nicolet ID5 attenuated total reflectance IR spectrometer operating at ambient temperature. The KBr pellets were used.

*Variable temperature PXRD under $CO_2$:*

Sample was loaded on to a 0.5 mm glass capillary and then evacuated by heating at 150 $^{o}$C for 12 hrs, then was backfilled with $CO_2$ at ~900 mbar pressure.

The capillary, while mounted in the measurement position in the X-ray diffractometer, was heated using a constant flow of hot air stream, temperature of which was continuously monitored using a K-type thermocouple and fed back to the electronic heater controller, which controlled the heater power to reach the set-point temperature. The thermocouple was placed in close to the capillary, without interfering with the path of the X-ray, to ensure that the actual temperature of the capillary was measured with good accuracy.

***3. Single crystal structure determination:***

Single-crystal data was collected on a Bruker SMART APEX four-circle diffractometer equipped with a CMOS photon 100 detector (Bruker Systems Inc.) and with a Cu Kα radiation (1.5418 Å). The incident X-ray beam was focused and monochromated using Microfocus (IμS). Crystal of **3**, **4** and **2*** were mounted on nylon Cryo loops with Paratone-N oil. Data of **3** and **2*** was collected at 100(2) K while the data of **4** was collected at 200(2) K. Data was integrated using Bruker SAINT software and was corrected for absorption using SADABS. Structure was solved by Intrinsic Phasing module of the Direct methods and refined using the SHELXTL 2014 software suite. All non-hydrogen atoms were located from iterative examination of difference F-maps following which the structure was refined using least-squares method. Hydrogen atoms were placed geometrically and placed in a riding model.

**Table S1**: Unit Cell Parameters for various polymorphic phases of ZnAtzOx.

| MOF | a (Å) | b(Å) | c(Å) | α | β | ϒ | Space group | Volume |
|---|---|---|---|---|---|---|---|---|
| 1 | 13.838 | 12.784 | 16.885 | 90° | 90° | 90° | Pbca | 2987 |
| 2* | 17.576 | 7.9026 | 10.347 | 90° | 100.21° | 90° | $P2_1/c$ | 1414.39 |
| 3 | 8.9818 | 13.8656 | 12.4104 | 90° | 105.360° | 90° | $P2_1/n$ | 1490.36 |
| 4 | 9.1387 | 13.614 | 12.551 | 90° | 104.80° | 90° | $P2_1/n$ | 1509.68 |

CCDC references:
2* = CCDC 1428296
3 = CCDC 1438585
4 = CCDC 1428298

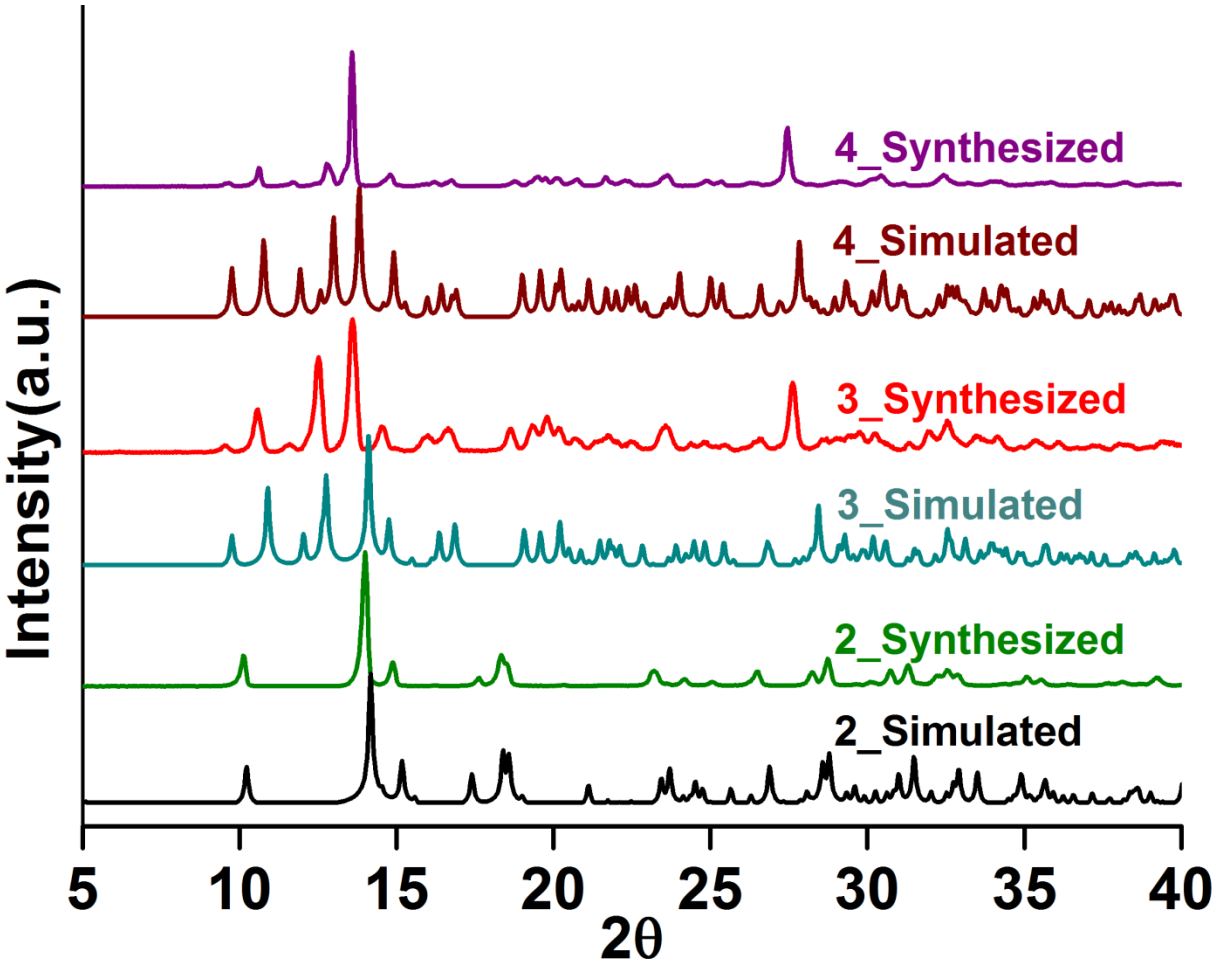


**Figure S1**: PXRD Comparison of simulated and as-synthesized for the polymorphic phases of ZnAtzOx.

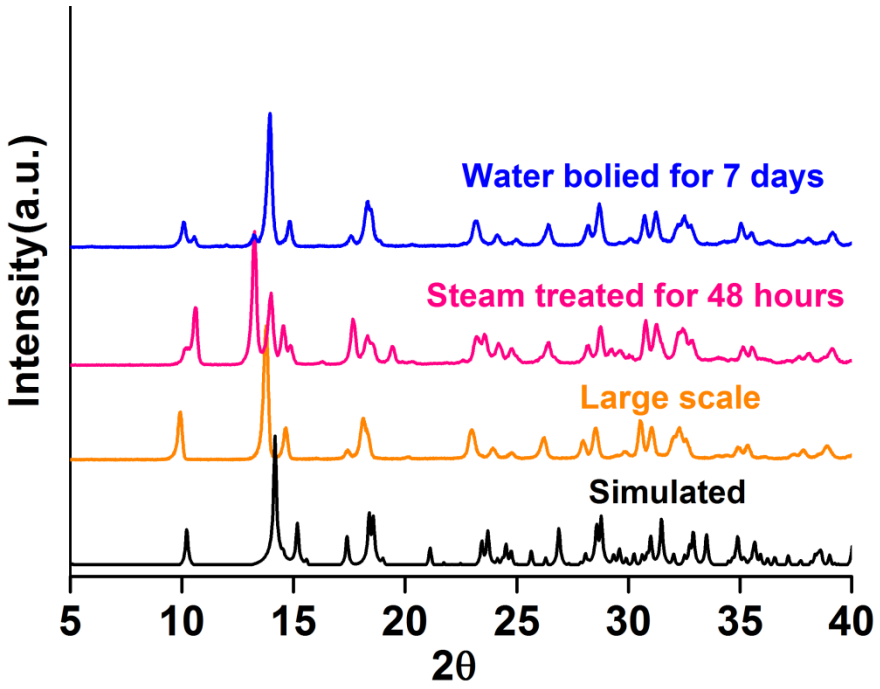


**Figure S2a:** Comparison of the PXRD patterns of phase **2** synthesized in mg and gm scales and also the water/ steam treated samples. Note: The changes in relative intensities is strongly dependent on extent of solvent inclusion.

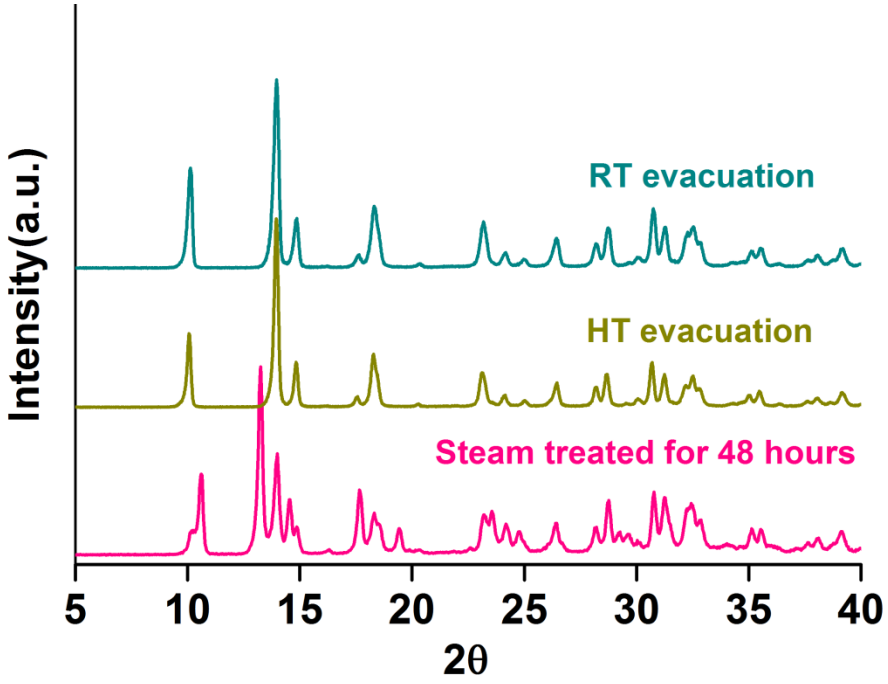


**Figure S2b:** Comparison of the PXRD patterns of phase **2** exposed to moisture, high temperature (HT) evacuated (150 $^{0}$C), low temperature (LT) evacuated. Note: The changes in relative intensities is strongly dependent on extent of solvent inclusion.

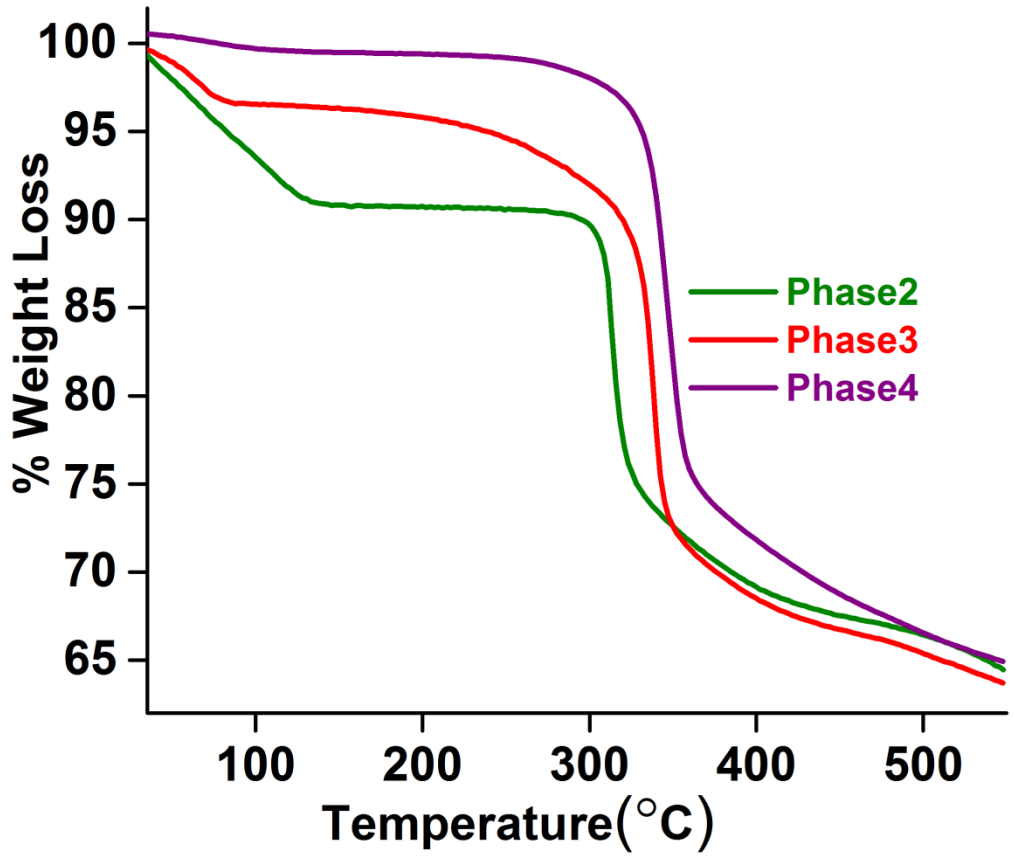


**Figure S3**: TGA curve for the different ZnAtzOx phases indicating good thermal stabilities.

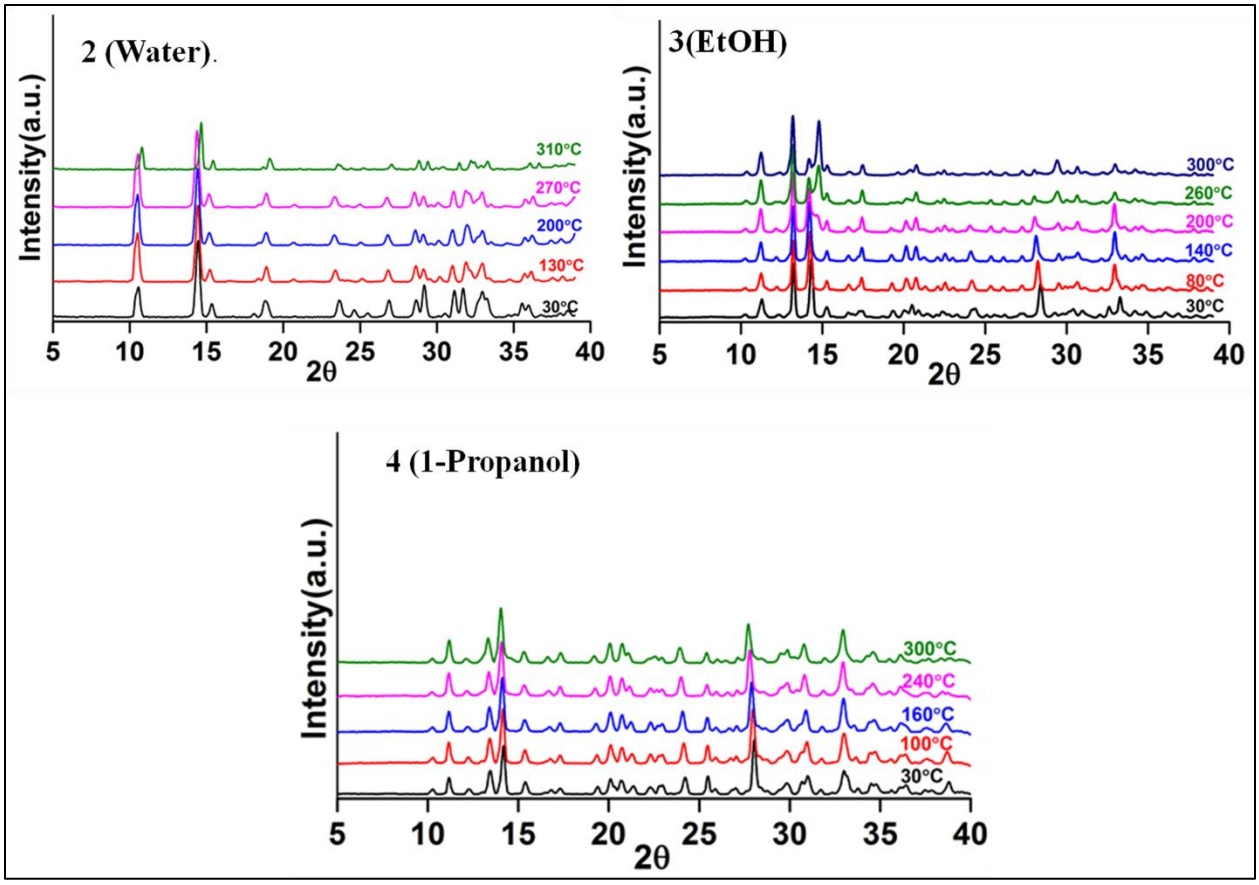


**Figure S4:** VTPXRD for showing complete retention of crystallinity to temperatures as high as 300 $^{o}$C. Also no thermally assisted phase changes are observed, except in case of **3** (EtOH), the resulting phase was not porous.

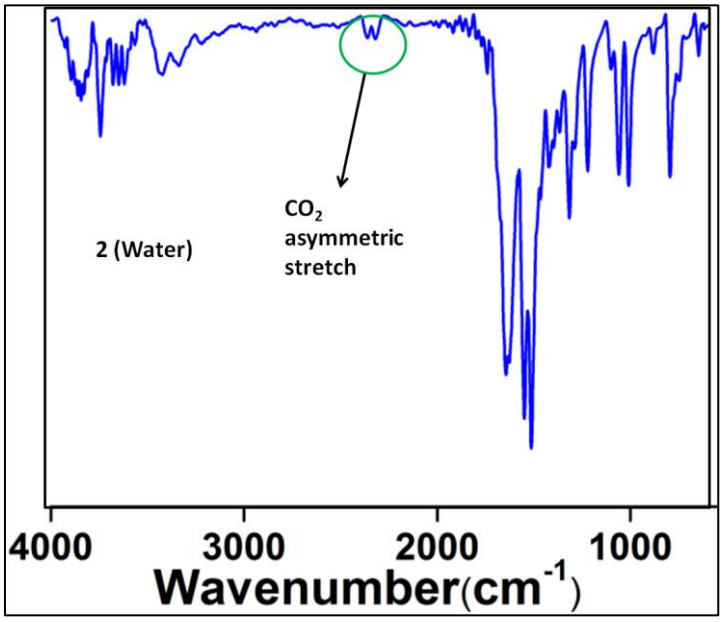


**Figrue S5:** Infra-red spectra of **2** showing the characteristic bands corresponding to oxalate and Atz units and in addition the bands due to $CO_2$ being adsorbed from air. The sample was not treated with any pure $CO_2$.

**Structural analysis: Porosity-structure correlations via a topological analysis.**

A feature that stands out during the comparison of the $CO_2$ uptakes of the different phases is their uptakes before the gate opening, i.e. in the low-pressure region of the isotherm. It can be seen that **2** has higher uptake even in the low pressure regime (0-200 mbar) compared to all the other phases, particularly the **1**, which itself shows remarkable low pressure $CO_2$ uptake.(*Vaidhyanathan et al., Science, 2010*) Now this is not due to any structural rearrangements under $CO_2$, but is inherent to the as-synthesized framework's structure. To correlate this low pressure $CO_2$ uptake to the structure, we have broken the structural building units into two components and have compared the differences between the phases based on these components. (i) the Atz layers (ii) the oxalate pillars. Atz layers are made up of $Zn_2Atz_2$ dimers, now within a layer these dimers are arranged in a non-coplanar fashion giving rise to puckering. We have defined a mean plane about each unique dimer and have compared the number of such unique dimers and the angles that the planes make between each other. From figure S6 it can immediately be seen that the most porous phase, **2** or **2***, has only one value for the angle and thus represents the most symmetrical arrangement close to a regular cubic topology. This has direct geometric implication on the openness of the structure.

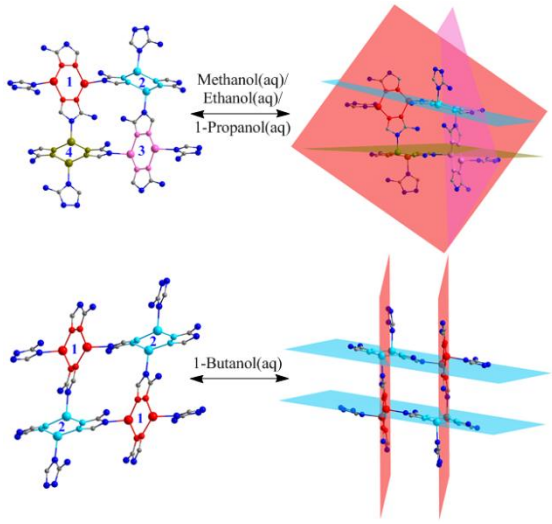


| Planes containing $Zn_2$-dimeric units | Angle between the planes | | |
|---|---|---|---|
| | Phase [1] Methanol(aq) | Phase [2] Ethanol(aq) | Phase [3] 1-Propanol(aq) |
| Red and Blue Planes | 86.661 | 84.743° | 67.865° |
| Blue and Pink Planes | 81.752 | 72.124° | 80.140° |
| Pink and Brown Planes | 86.661 | 80.011° | 67.865° |
| Brown and Red Planes | 81.752 | 72.445° | 80.140° |

(a)

| Planes containing $Zn_2$-dimeric units | Angles between the planes in 1-Butanol Phase/ Water phase |
|---|---|
| Red and Blue Planes | 80.145° |
| Blue and Red Planes | 80.145° |

(b)

**Figure S6:** Planes containing $Zn_2Atz_2$-dimeric units of the ZnAtzOx Phases. Right: Figure (a) represents the planes containing these dimers and the graphical representation of the angle between them. Left: Table listing the angles between the dimer containing planes for the different phases. Note, each different dimer and the plane have been color coded.

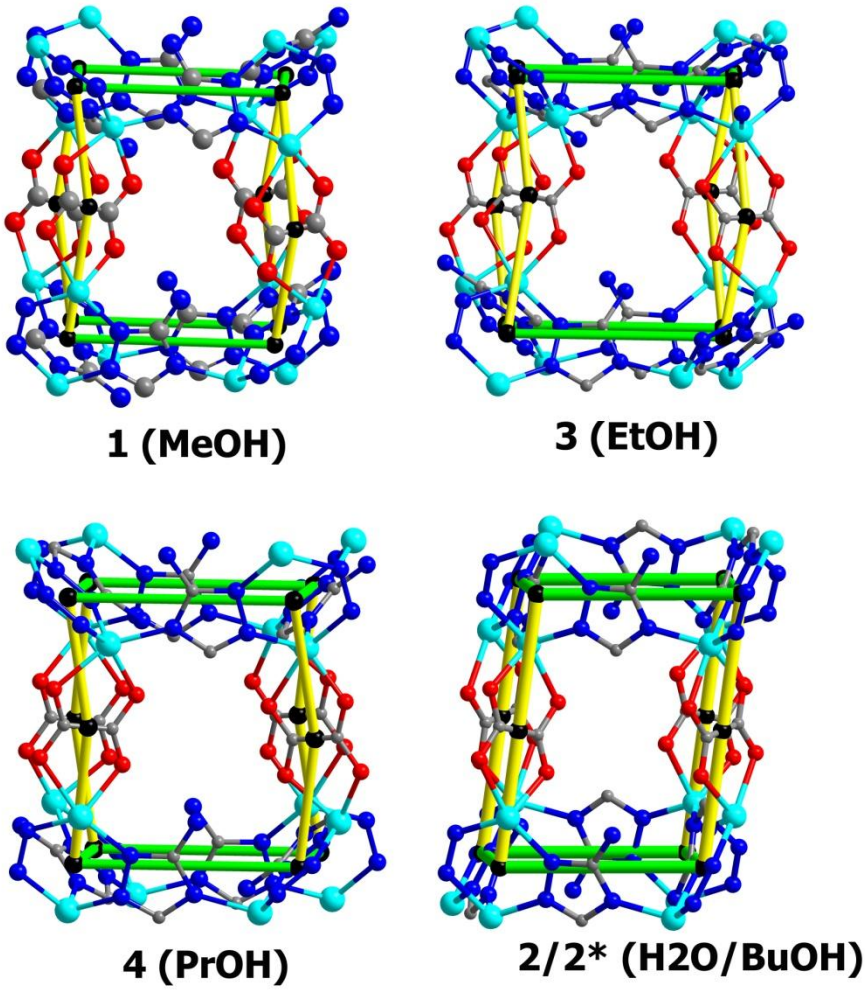


**Figure S7:** The cavities in **1**, **2***, **3**, **4** have been shown and the overlaying 6-connected topology represents the cavities as distorted cubes (green-yellow). As can be seen, the shape of the cubes is determined by the tilt angle of the oxalate pillars and the puckering of the Atz layers.

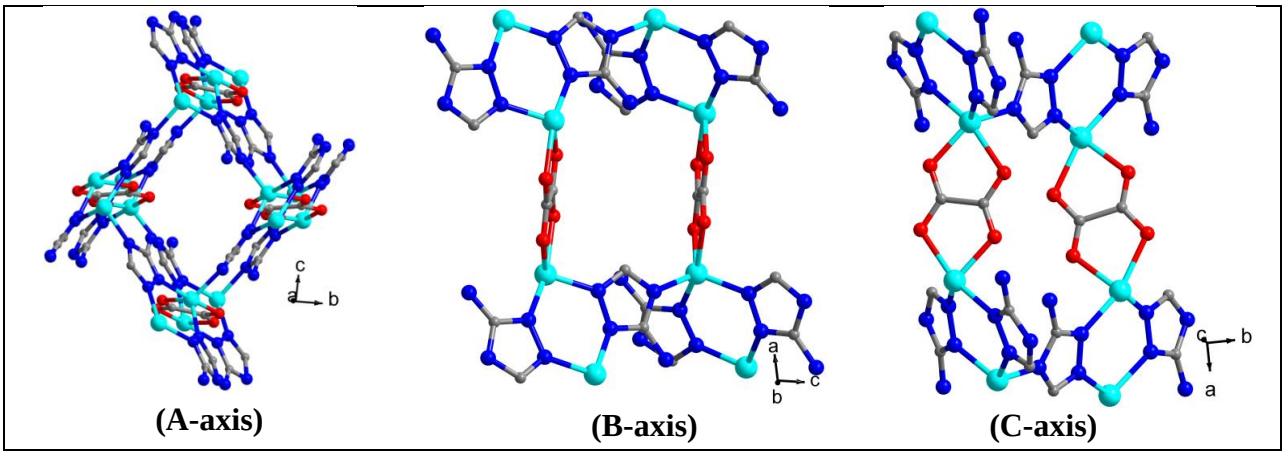


**Figure S8**: View along the three crystallographic axes for **2/2***.

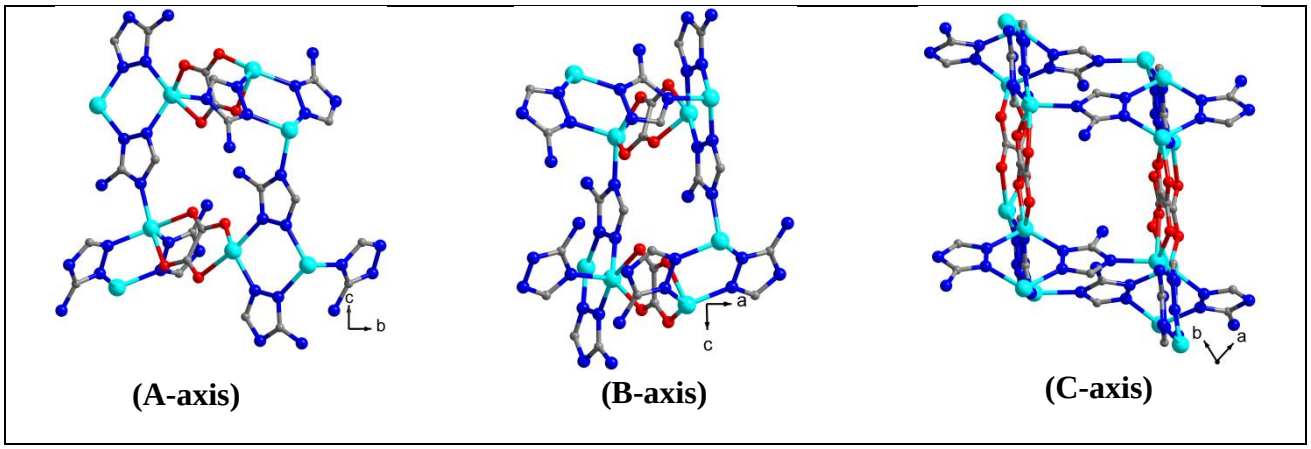


**Figure S9**: View along the three crystallographic axes for **3**.

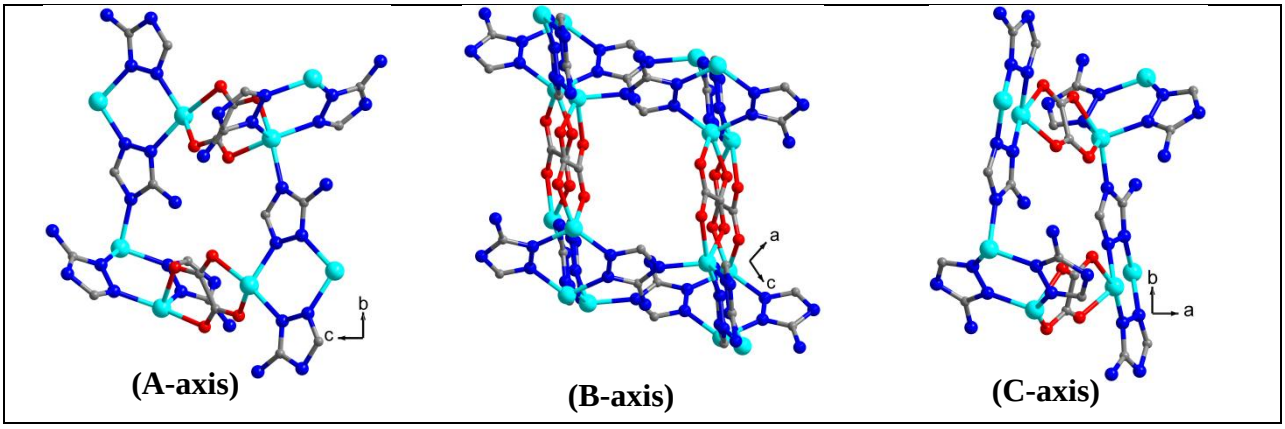


**Figure S10**: View along the three crystallographic axes for **4**.

## Adsorption Analysis:

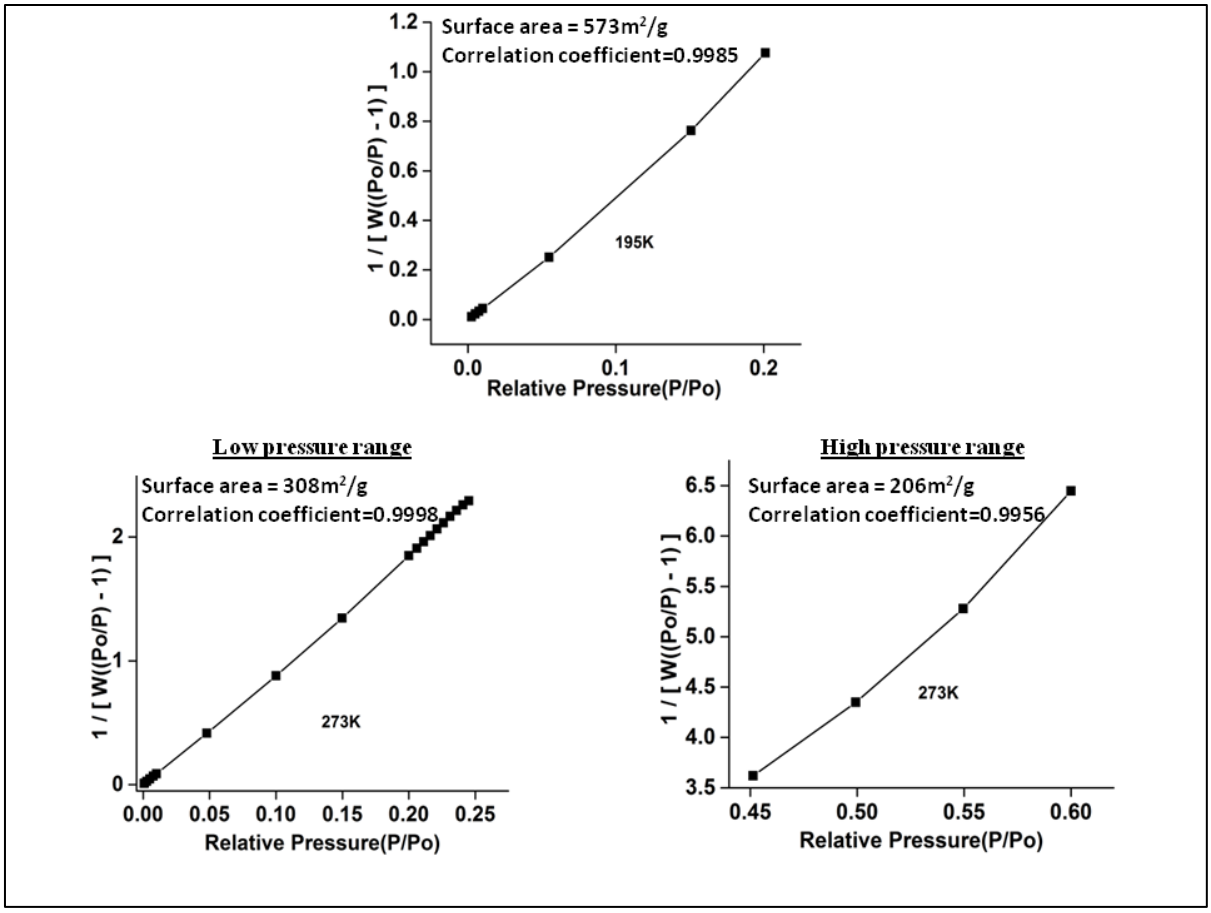


**Figure S11:** BET surface area fit for **2** (top) from 195K $CO_2$ Isotherm and (bottom) 273 K $CO_2$ isotherm.

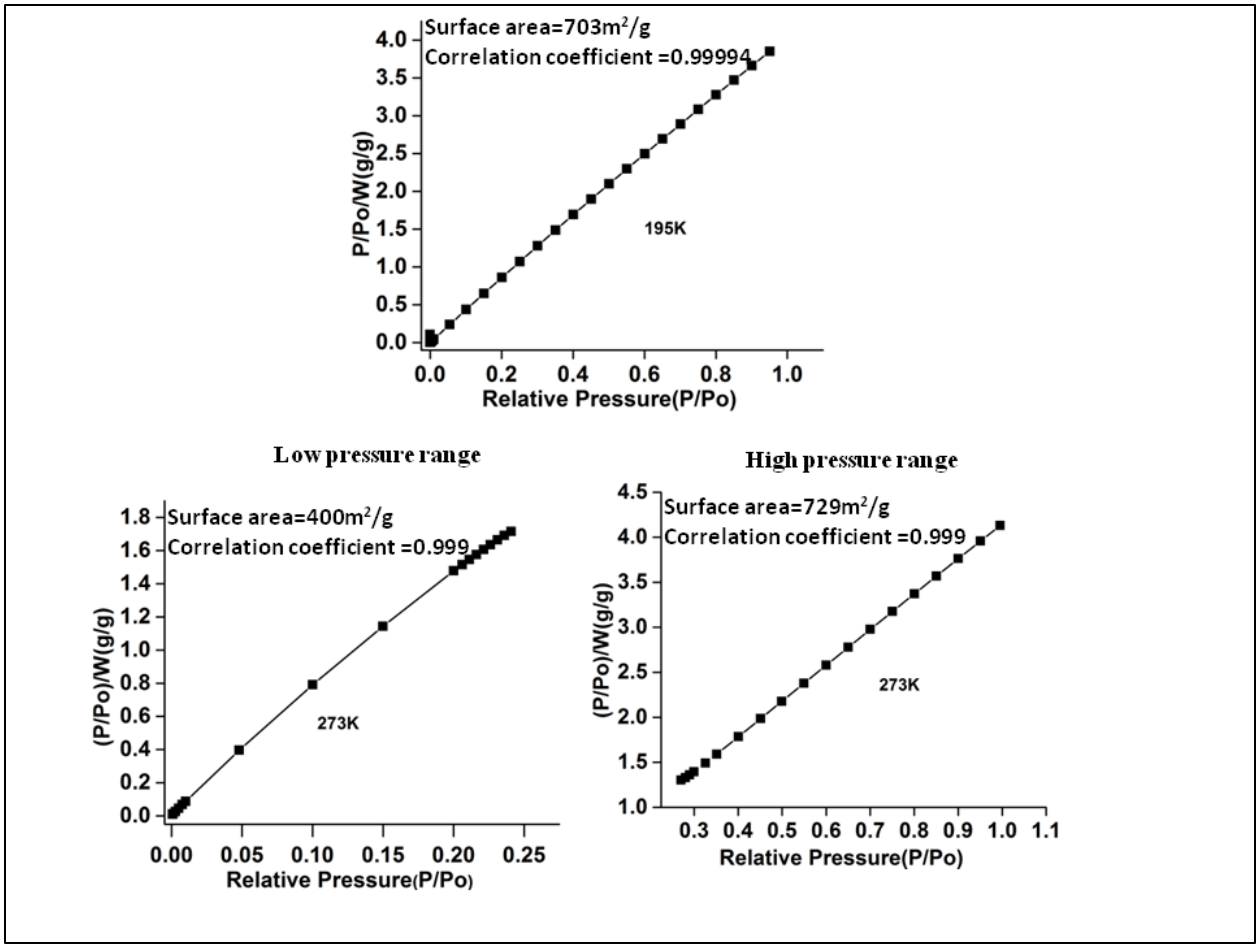


**Figure S12**: Langmuir surface area fit for **2** (top) from 195 K $CO_2$ isotherm and (bottom) 273 K $CO_2$ isotherm.

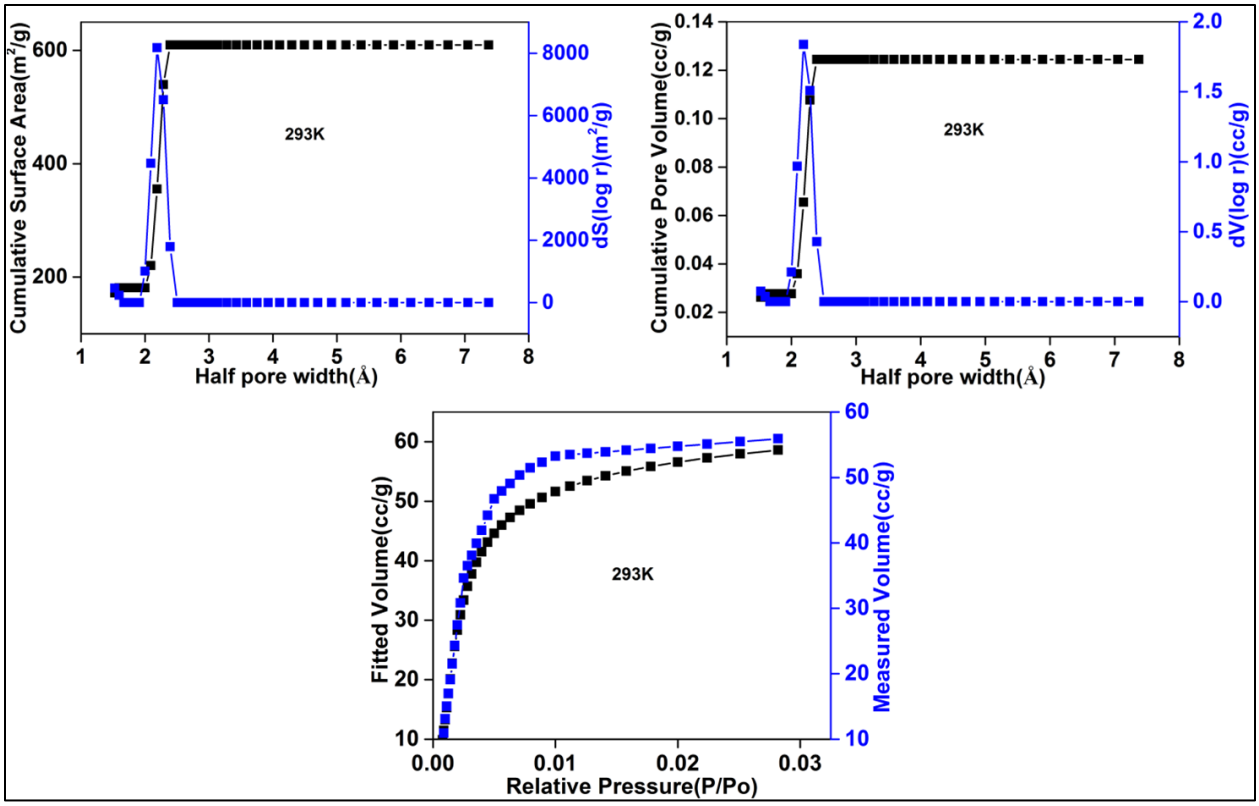


**Figure S13**: DFT pore size evaluations and fit comparisons for **2**. Note: Due to the stepped nature of the 273 K isotherm DFT (273 K, Carbon) model could not be fitted to it. The 195 K data without steps is too far away from the 273 K model, hence the model has been fitted to 293 K data.

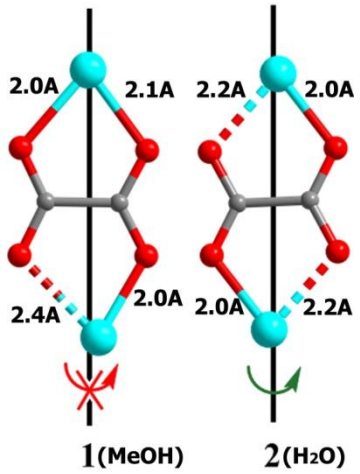


**Figure S14:** Comparison of the Zinc-oxalate units in **1** and **2/2***. Despite the presence of relatively longer Zn-O bond, **1**, does not show any gate opening (flexibility), while the symmetrically positioned weaker Zn-O bonds (2.2 Å) in **2** could be key to favoring the spindle like rotation motion of the oxalate units giving rise to gate opening. Note: Other phases, **3** (EtOH) and **4** (PrOH) do have Zn-O bonds longer than 2.2 Å, again they are not symmetrically (diagonally) positioned.

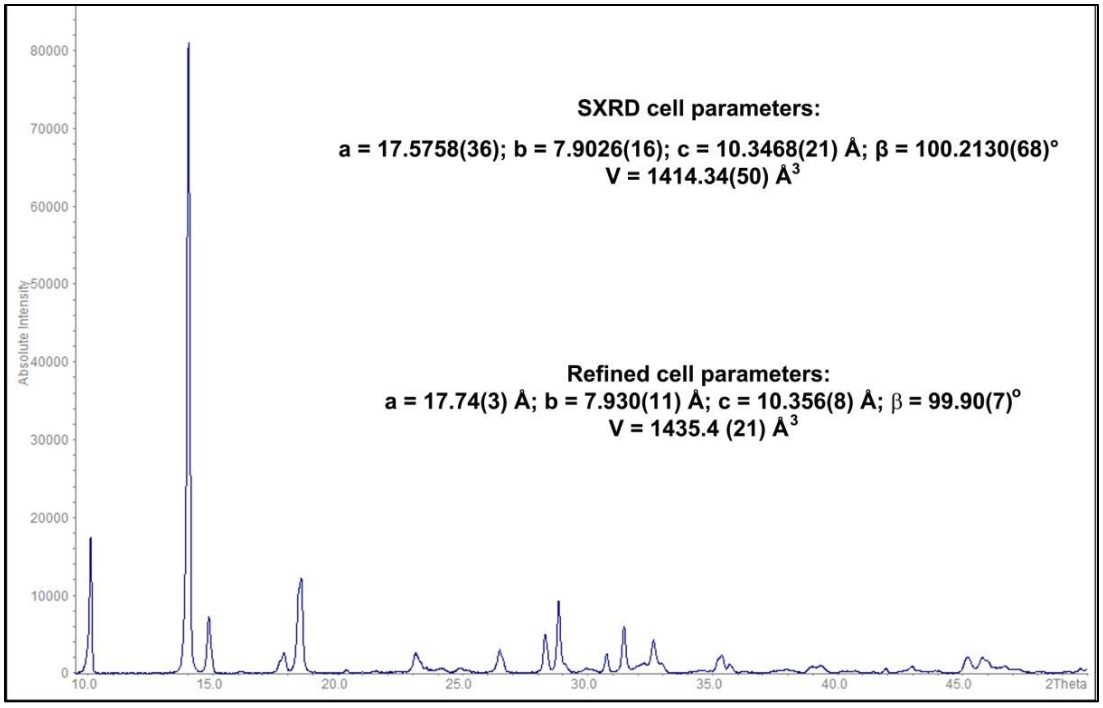


**Figure S15a:** PXRD of a sample that was maintained at 900 mbar pressure of $CO_2$ in a capillary.

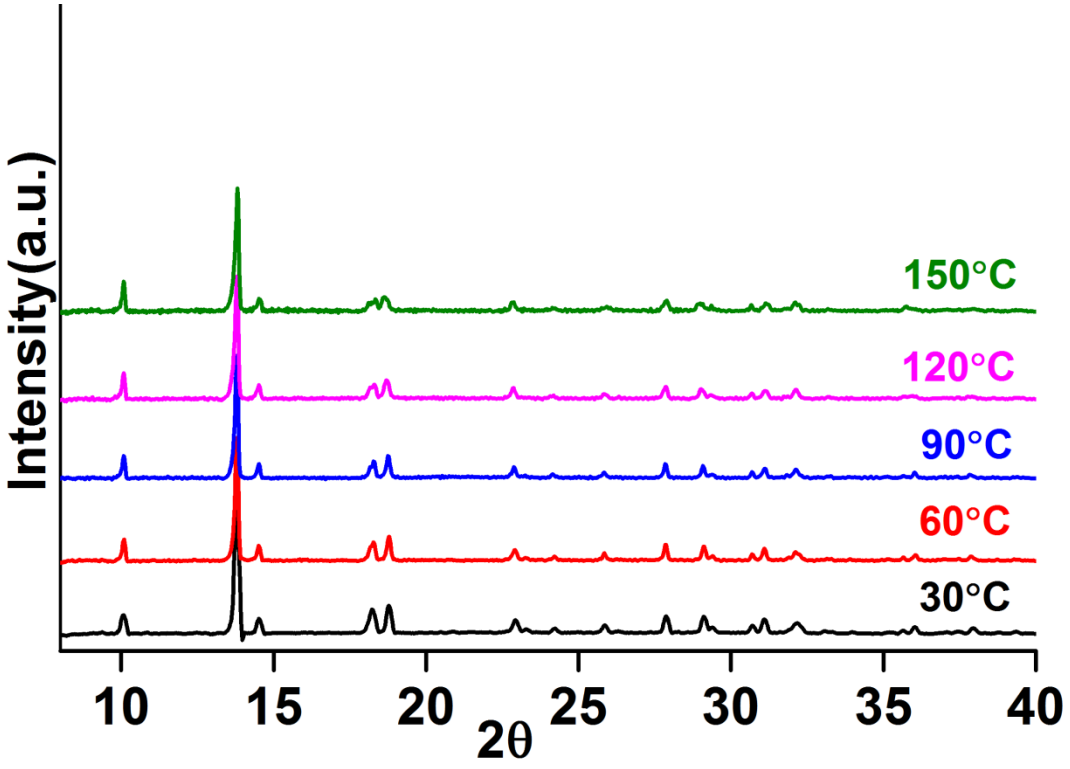


**Figure S15b:** PXRD of a sample that was maintained at 900 mbar pressure of $CO_2$ in a capillary at different temperatures.

**Dual site Langmuir-Freundlich modeling of $CO_2$ isotherms of 2:**

The dual site model was carried out using the 273K adsorption branch.

Fit parameters:

$$q \equiv q_A + q_B = \frac{q_{sat,A} b_A p^2}{1 + b_A p^2} + \frac{q_{sat,B} b_B p}{1 + b_B p}$$

$$b_A = b_{A0} \exp\left(\frac{E_A}{RT}\right); \quad b_B = b_{B0} \exp\left(\frac{E_B}{RT}\right);$$

$b_{A0}$ = 4.78 x $10^{-13}$ $Pa^{-2}$
$b_{B0}$ = 8.09 x $10^{-12}$ $Pa^{-2}$
$E_A$ = 46.46 kJ $mol^{-1}$
$E_B$ = 32.65 kJ $mol^{-1}$
$q_{sat,A}$ = 2.12 mol $kg^{-1}$
$q_{sat,A}$ = 6.39 mol $kg^{-1}$

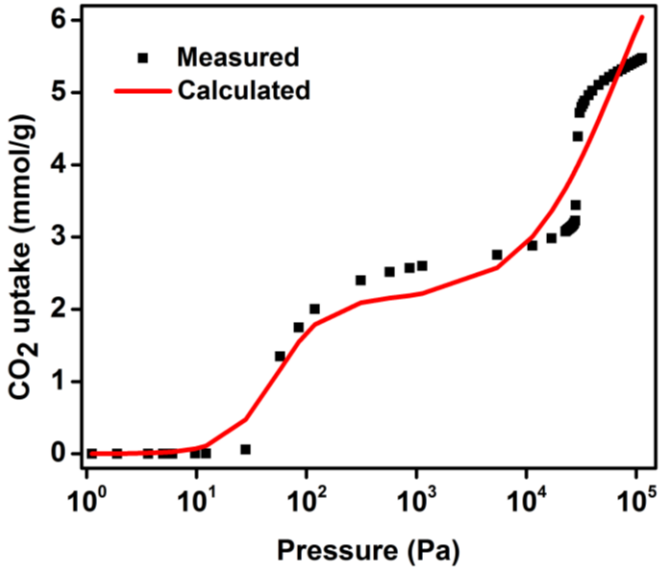


**Figure S16:** Log plot of the Dual site Langmuir-Freundlich model fitted for the 273K $CO_2$ adsorption branch.

**Table S2:** $CO_2$ adsorption isotherm at 273K showing measured and calculated uptakes from a dual site Langmuir-Freundlich model

| Pressure (Pascal) | Amount adsorbed (mmol/g) | Calculated Amount adsorbed |
|---|---|---|
| 1.11972 | 0.000232 | 0.00032323 |
| 1.89286 | 0.000388 | 0.00293759 |
| 3.63909 | 0.001138 | 0.01051918 |
| 4.95876 | 0.001777 | 0.0192921 |
| 6.02516 | 0.002286 | 0.02824791 |
| 9.70424 | 0.004379 | 0.07127763 |
| 12.21028 | 0.005451 | 0.11044401 |
| 28.03299 | 0.061107 | 0.47487415 |
| 57.59893 | 1.349134 | 1.16629683 |
| 85.312 | 1.749272 | 1.54820701 |
| 118.8769 | 2.002335 | 1.78703956 |
| 311.0689 | 2.398433 | 2.09059692 |
| 571.8303 | 2.517281 | 2.15464673 |
| 865.7169 | 2.571411 | 2.19052754 |
| 1131.49 | 2.600661 | 2.21703078 |
| 5439.466 | 2.755094 | 2.57645091 |
| 11345.24 | 2.879379 | 3.00290301 |
| 16978.3 | 2.981254 | 3.35613001 |
| 22667.29 | 3.077513 | 3.66966756 |
| 23351.49 | 3.092728 | 3.70482487 |
| 23931.03 | 3.105879 | 3.7342069 |
| 24492.24 | 3.118643 | 3.76231926 |
| 25073.78 | 3.131161 | 3.79110356 |
| 25626.57 | 3.144192 | 3.81814238 |
| 26197.66 | 3.158746 | 3.8457536 |
| 26745.27 | 3.174661 | 3.8719258 |
| 27289.63 | 3.193929 | 3.89765309 |
| 27789.74 | 3.224946 | 3.92103915 |
| 28238.63 | 3.441951 | 3.94182874 |
| 29364.32 | 4.392018 | 3.99314446 |
| 30642.98 | 4.719813 | 4.05005236 |
| 31790.53 | 4.798821 | 4.09991834 |
| 32806.13 | 4.844228 | 4.14312949 |
| 33971.56 | 4.885201 | 4.19168385 |
| 36905.26 | 4.964237 | 4.30925951 |

| | | |
|---|---|---|
| 39813.83 | 5.024152 | 4.41967423 |
| 45398.78 | 5.105884 | 4.6162006 |
| 51135.2 | 5.167951 | 4.7993246 |
| 56580.44 | 5.214911 | 4.95790172 |
| 62270.4 | 5.255844 | 5.10974633 |
| 67986.75 | 5.290705 | 5.24976323 |
| 73657.78 | 5.320063 | 5.37772526 |
| 79341.08 | 5.347433 | 5.49627008 |
| 85043.16 | 5.373357 | 5.60652104 |
| 90690.04 | 5.39667 | 5.70803465 |
| 96360.24 | 5.418129 | 5.80306892 |
| 102027 | 5.439214 | 5.89181804 |
| 107728.4 | 5.459737 | 5.9754255 |
| 112801.5 | 5.478045 | 6.0454546 |

**Virial Analysis for evaluation of Heat of Adsorption (HOA) for $CO_2$ in 2:**

HOA calculations employing virial model proved extremely difficult owing to the stepped nature of the isotherm. However, a two site fit could be carried out and it yielded an HOA of 60kJ $mol^{-1}$ for the low zero-loading adsorption sites, while it presented a value of 46kJ $mol^{-1}$ for the second site. This is much higher than the values obtained from the dual site model discussed earlier. We remark, for this unusual gate opening case in an ultra-microporous rigid framework, the dual site model seemed to be more realistic. This is because comparing the abruptness of the low pressure $CO_2$ uptake between **1**(MeOH) and **2**(Water), it can be expected that **2** would have relatively higher interactions, but is unlikely to be possessing an interaction that is 20kJ $mol^{-1}$ higher for **2**. Or in other words, the initial slope of $CO_2$ adsorption isotherm would have been expected to be much steeper for **2** if it had to have an HOA as high as 60kJ $mol^{-1}$.

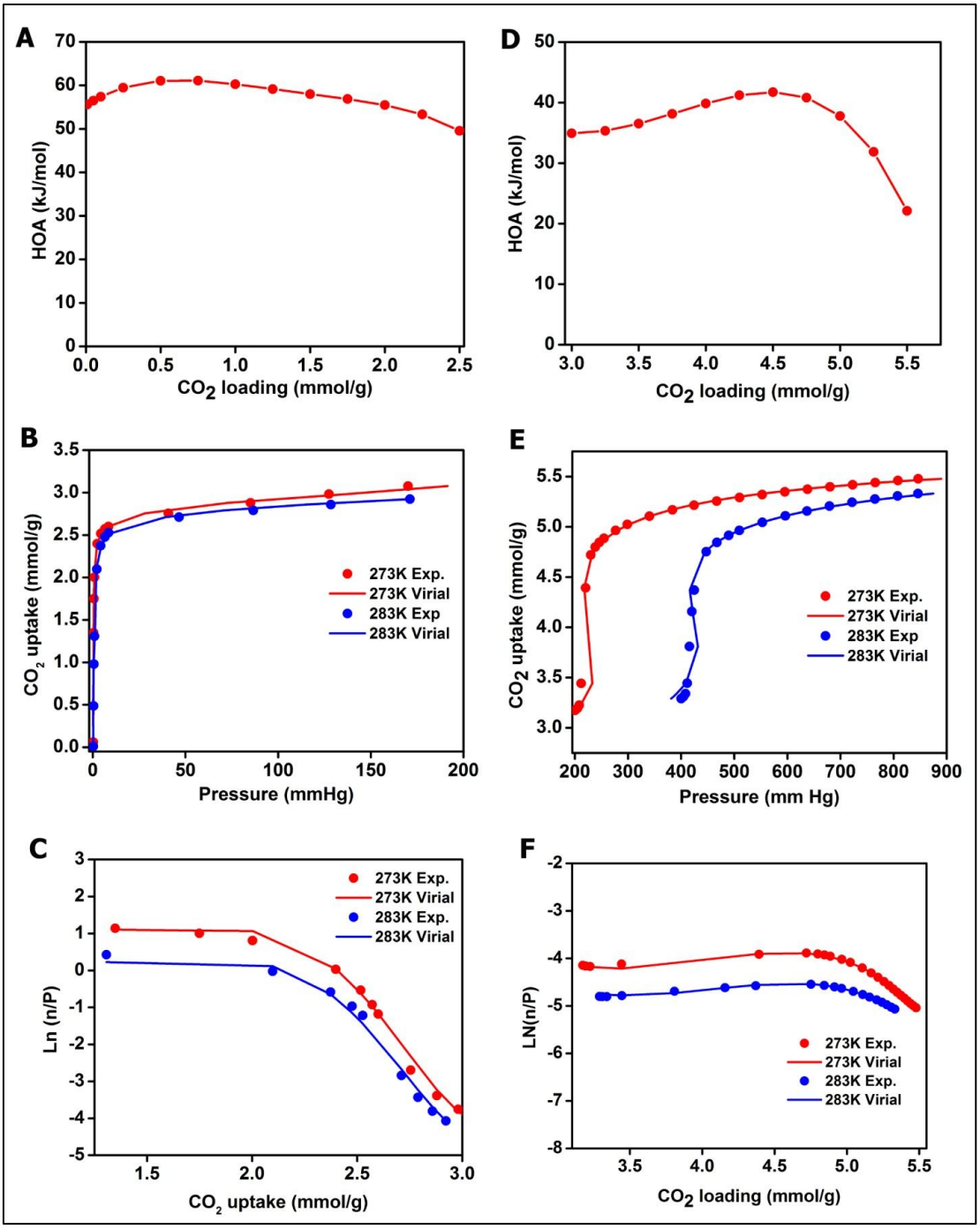


**Figure S17:** HOA plots and associated Virial analysis for **2**.

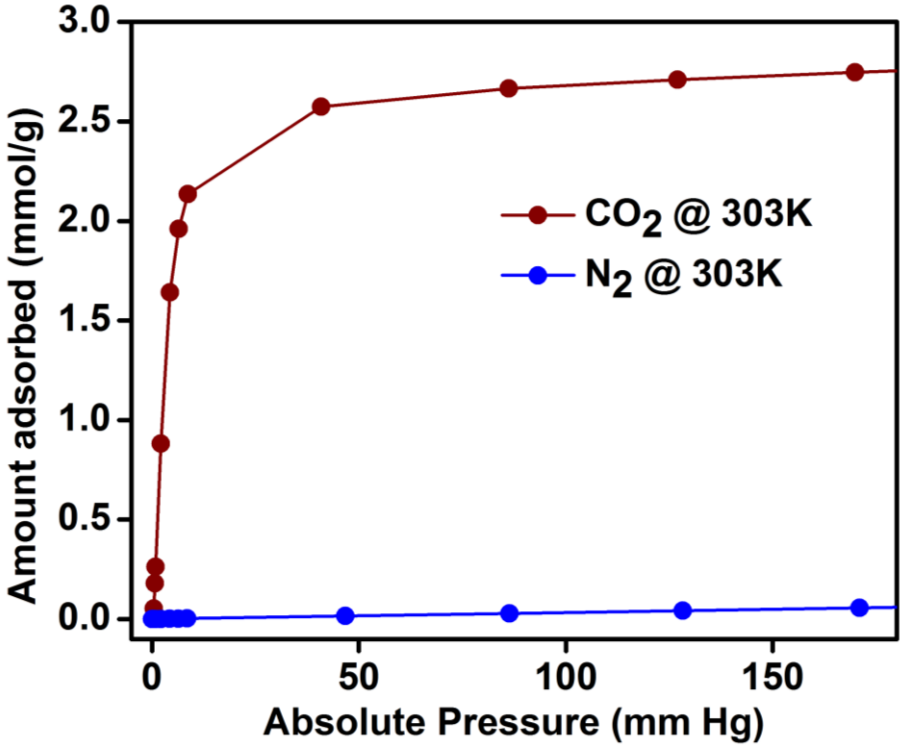


**Figure S18a:** An initial slope comparison of the $CO_2$ and $N_2$ uptakes in **2** showing the high apparent selectivity for $CO_2$.

**Ideal Adsorbed Solution Theory (*IAST*):**

IAST calculations were undertaken as described by Prausnitz *et al.*[S1] The isotherms were fitted using Dual site Langmuir or modified Dual site Langmuir model by solving the Langmuir equation using the solver function in Microsoft Excel following a similar protocol to Keller *et al.*[S2] The selectivity equation is provided below.

*Selectivity:*

$$S_{1,2} = \frac{q_1/q_2}{P_1/P_2}$$


(S1) Myers, A. L.; Prausnitz, J. M. *AIChE J.* **1965**, *11*, 121–127.
(S2) Kemmer, G.; Keller, S. *Nat. Protoc.* **2010**, *5*, 267–81.


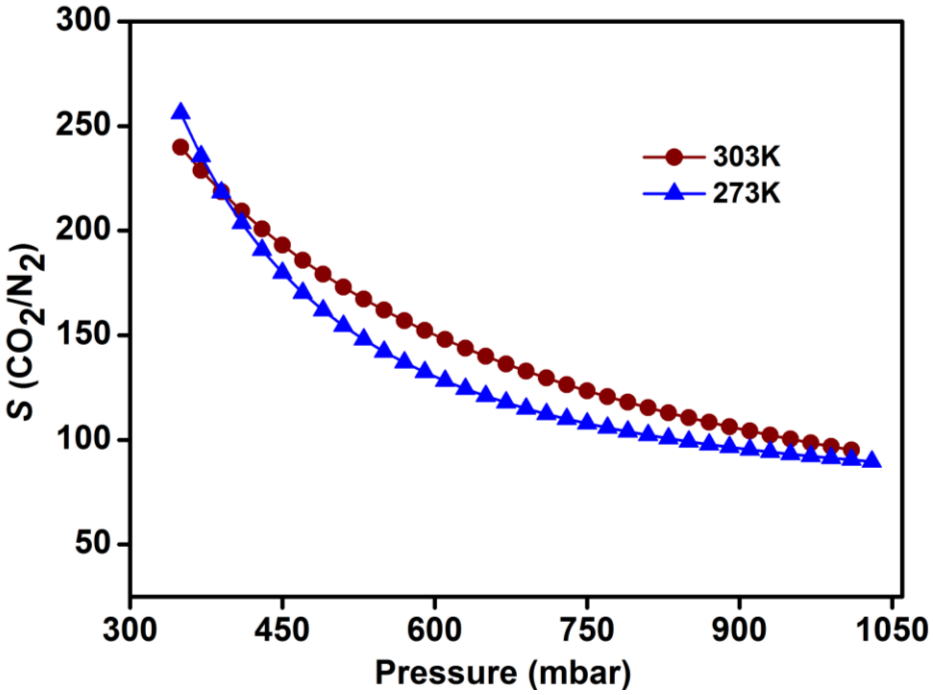


**Figure S18b:** $CO_2/N_2$ selectivities calculated using IAST methods.

**Table S3:** Chart showing the $CO_2$ and $N_2$ uptakes of different ultra-microporous MOFs at pressures relevant to vacuum swing adsorption based $CO_2/N_2$ separation from flue gas ($85N_2$:$15CO_2$) compositions.*

| Metal Organic framework | **$CO_2$ Uptakes (mmol/g) (0.15bar)** | **$N_2$ Uptakes (mmolg) (0.75bar)** | **Temperature (Kelvin)** | **Reference** |
|---|---|---|---|---|
| UTSA-16 | 2.64 | 0.05 | 296 | S3 |
| SIFSIX-3-Zn | 2.43 | 0.14 | 298 | 11c* |
| SIFSIX-3-Cu-i | 2.38 | 0.16 | 298 | 11c* |
| $Zn_2(atz)_2(ox)$ | 2.05 | -- | 298 | 11b* |
| MAF-66 | 1.25 | 0.030 | 298 | 4a* |
| SIFSIX-3-Cu | 0.31 | 0.10 | 298 | S4 |
| [Cu(bpy-1)2(SiF6)] | 0.69 | 0.15 | 298 | S5 |
| SNU-50 | 0.68 | -- | 298 | S6 |
| ZnATzOx_Water, **2**, (This work) | **2.70** | **0.1** | **303** | **This work** |

* these references are included in the main text.

**References for table S3:**

S3: S. Xiang, Y. He, Z. Zhang, H. Wu, W. Zhou, R. Krishna and B. Chen, *Nat. Commun.*, 2012, **3**, 954.
S4: O. Shekhah, Y. Belmabkhout, Z. Chen, V. Guillerm, A. Cairns, K. Adil and M. Eddaoudi, *Nat. Comm.*, 2014, **5**, 4228.
S5: S. D. Burd, S. Ma, J. A. Perman, B. J. Sikora, R. Q. Snurr, P. K. Thallapally, J. Tian, L. Wojtas and M. J. Zaworotko, *J. Am. Chem. Soc.*, 2012, **134**, 3663–3666.
S6: T. K. Prasad, D. H. Hong and M. P. Suh, *Chem.Eur. J.*, 2010, **16**, 14043–14050.

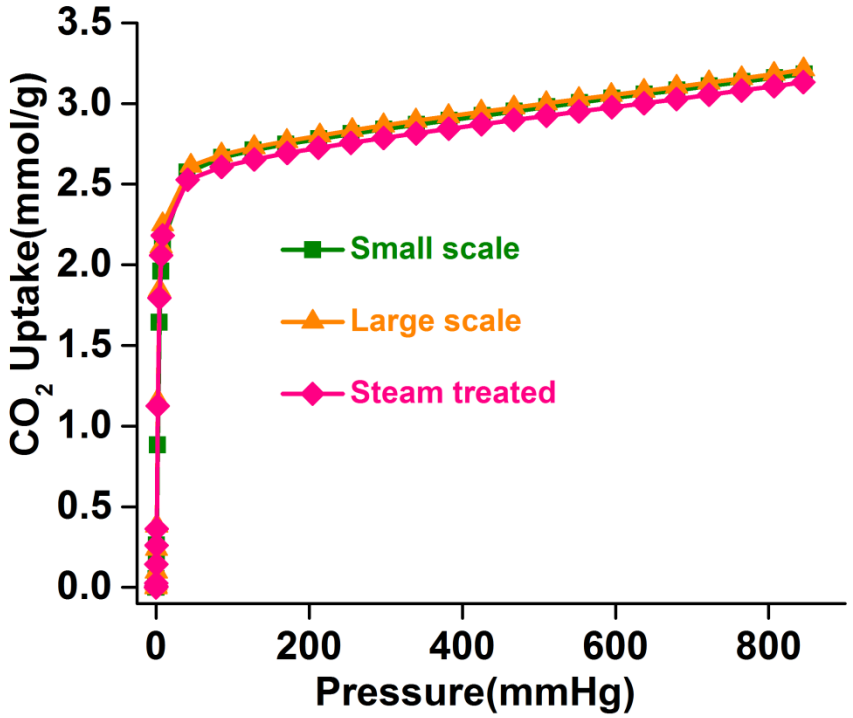


**Figure S19:** $CO_2$ adsorption comparison for **2** under various conditions at RT.

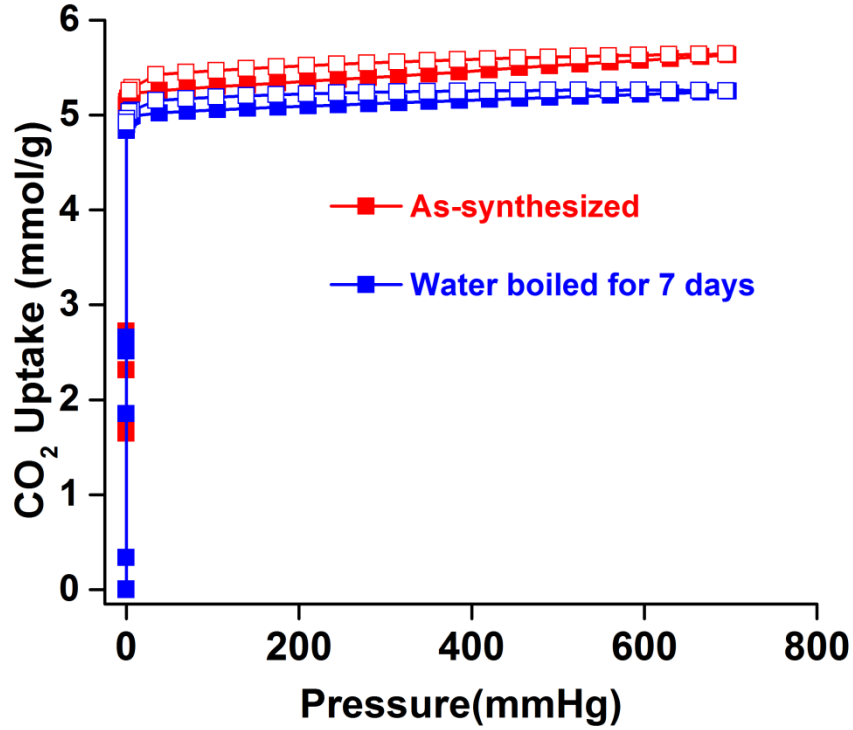


**Figure S20:** $CO_2$ adsorption for water boiled phase **2** at 195 K. About 6% loss is observed. However, when this same sample was again subjected to water boiling (24 hrs) no further loss of uptake was observed.